Energy & Environmental Science

PAPER

View Article Online
View Journal | View Issue

Cite this: *Energy Environ. Sci.*, 2017, **10**, 2616

An efficient organic magnesium borate-based electrolyte with non-nucleophilic characteristics for magnesium–sulfur battery†

Aobing Du, ‡[ab] Zhonghua Zhang,‡[c] Hongtao Qu,[a] Zili Cui,[a] Lixin Qiao,[c] Longlong Wang,[a] Jingchao Chai,[a] Tao Lu,[a] Shanmu Dong,[a] Tiantian Dong,[a] Huimin Xu,[c] Xinhong Zhou[c] and Guanglei Cui *[a]

Received 13th August 2017,
Accepted 16th November 2017

DOI: 10.1039/c7ee02304a

rsc.li/ees

Two-electron transfer chemistry based on earth-abundant Mg and S offers great possibilities of delivering higher energy density than current Li-ion technology. The development of non-nucleophilic electrolytes that reversibly and efficiently plate and strip Mg is believed to be a major obstacle to the implementation of this divalent battery technology. In this study, we present a new type of organic magnesium borate-based electrolyte that primarily comprises tetrakis(hexafluoroisopropyl)borate anions $[B(HFP)_4]^-$ and solvated cations $[Mg_4Cl_6(DME)_6]^{2+}$, which was synthesized *via* a facile *in situ* reaction of tris(hexafluoroisopropyl)borate $[B(HFP)_3]$, $MgCl_2$ and Mg powder in 1,2-dimethoxyethane (DME). Rigorous analyses including NMR, mass spectroscopy and single-crystal XRD were conducted to identify the equilibrium species in the abovementioned solution. The as-prepared Mg-ion electrolyte exhibited unprecedented Mg plating/stripping performance, such as high anodic stability up to 3.3 V (*vs.* Mg/Mg^{2+}), high ionic conductivity of 5.58 mS cm^{-1}, a low overpotential of 0.11 V for plating processes and Coulombic efficiencies greater than 98%. By virtue of the non-nucleophilic nature of this electrolyte, a fully reversible Mg/S battery was constructed that displayed an extremely low overpotential of 0.3 V and a high discharge capacity of up to 1247 mA h g^{-1} and yielded a specific energy of approximately 1200 W h kg^{-1} (10 times higher that of the Chevrel benchmark) based on the weight of active sulfur. More significantly, commonly used sulfur-carbon nanotube (S-CNTs) cathodes with S contents of 80 wt% and S loadings of 1.5 mg cm^{-2} were demonstrated to withstand more than 100 cycles without obvious capacity decay and to enable fast conversion processes, which achieved a charging current rate of up to 500 mA g^{-1}. Our findings convincingly validate the pivotal role of the newly designed non-nucleophilic Mg-ion electrolyte for practical Mg/S battery chemistry.

Broader context

As regards the demand for energy storage batteries, higher energy density and safer properties have been imperative targets with the rapid market expansion of electric vehicles and grid-scale storage systems. Although Li/S batteries have been the focus of research in energy storage systems and have made significant progress, the problem of dendrite formation with lithium metal anodes is still difficult to address fundamentally. In contrast, Mg anodes inherently possess superior resistance to dendrite growth and low cost (about 30 times cheaper than Li). Two-electron transfer chemistry based on earth-abundant Mg and S will offer significant prospects for application in the field of large-scale energy storage. Nevertheless, the development of Mg/S battery systems has been restricted owing to the lack of suitable non-nucleophilic magnesium electrolytes. Here, we report an organic magnesium borate-based electrolyte with non-nucleophilic characteristics for Mg/S batteries, of which the equilibrium species mainly comprise solvated cations $[Mg_4Cl_6(DME)_6]^{2+}$ and tetrakis(hexafluoroisopropyl)borate anions $[B(HFP)_4]^-$. This magnesium electrolyte with tetracoordinated $[B(HFP)_4]^-$ anions derived from the tetrahedral structure of boron oxide is stable to magnesium metal anodes and exhibits excellent electrochemical properties. It is worth mentioning that the performance of Mg/S batteries with this electrolyte is the best of those reported in the literature to date. Our work will be a critical step in promoting the practical applications of Mg/S batteries with high energy density.

[a] *Qingdao Industrial Energy Storage Research Institute, Qingdao Institute of Bioenergy and Bioprocess Technology, Chinese Academy of Sciences, Qingdao 266101, P. R. China. E-mail: cuigl@qibebt.ac.cn; Fax: +86-532-80662746; Tel: +86-532-80662746*

[b] *University of Chinese Academy of Sciences, Beijing 100190, P. R. China*

[c] *College of Chemistry and Molecular Engineering, Qingdao University of Science and Technology, Qingdao 266042, P. R. China*

† Electronic supplementary information (ESI) available. CCDC 1545755 and 1582813–1582815. For ESI and crystallographic data in CIF or other electronic format see DOI: 10.1039/c7ee02304a

‡ Aobing Du and Zhonghua Zhang contributed equally.

Introduction

To satisfy the demand for advanced energy storage, attractive choices include alkaline or alkaline earth metal anodes owing to their high theoretical volumetric capacities; for example, the volumetric capacities of lithium, sodium and magnesium (Mg) are 2062, 1128 and 3832 mA h cm^{-3}, respectively.[1–4] Among these metal anodes, Mg inherently possesses incomparably superior properties: resistance to dendrite growth, higher volumetric capacity, earth-abundance (the fifth most abundant element in the Earth's crust) and low cost (about 30 times cheaper than Li).[5–8] The first prototype of a rechargeable magnesium battery was demonstrated by Aurbach *et al.* in 2000 with unprecedented cycling stability.[9] However, this system is commonly known to provide unsatisfactory energy density owing to its low operating voltage of $\sim$1.1 V and low specific capacity of $\sim$100 mA h g^{-1}.[10]

As far back as 2008, Armand and Tarascon drew the conclusion that redox chemistries that couple high-capacity cathode materials, including sulfur and oxygen, and Mg anodes are a promising alternative to current Li-ion technologies.[11] Theoretically, Mg/S batteries have a high energy density of 1722 W h kg^{-1}, which is over four times that of commercial $LiCoO_2$/graphite chemistry.[5,12] In 2011, Muldoon *et al.* demonstrated the first proof-of-concept Mg–S battery, which employed newly developed solutions of non-nucleophilic hexamethyldisilazide magnesium chloride (HMDSMgCl).[5] The anionic species ($HMDS_xAlCl_{4-x}^-$, $0 \leq x \leq 4$) in this non-nucleophilic electrolyte opened the door to the development of various Mg-conductive electrolytes for measuring the performance of Mg/S batteries by virtue of their compatibility with electrophilic sulfur. Fichtner *et al.* optimized the physicochemical properties of the non-nucleophilic Mg-HMDS-based electrolyte by using a new synthetic method and binary solvents of glyme and ionic liquids.[13] Mg/S batteries displayed improved cycling stability when these novel electrolytes were employed. Wang *et al.* attempted to add LiTFSI to the non-nucleophilic Mg-HMDS-based electrolyte in order to enhance the reversibility of Mg/S chemistry.[12] Over 30 discharging/charging cycles have been achieved using this system. Besides, some electrolytes based on electroactive Mg salts, namely, $[Mg(THF)_6][AlCl_4]_2$ or $Mg(TFSI)_2$, have also been used to examine the performance of Mg/S batteries.[14,15] Unfortunately, none of these displayed the expected capacity and cycling performance of those that used the Mg-HMDS-based electrolyte. More recently, our group employed a boron-centered anion/magnesium (BCM)-based electrolyte using another non-nucleophilic anionic species, namely, the tetrakis(hexafluoroisopropyl)borate anion, in Mg/S batteries, which exhibited a specific capacity of $\sim$1000 mA h g^{-1} for 30 cycles.[16] Zhao-Karger *et al.* straightforwardly synthesized magnesium tetrakis(hexafluoroisopropyloxy)borate salts and utilized them in Mg/S cells, which exhibited an acceptable capacity and cycle life.[17]

To sum up, the development of Mg/S batteries is still in its infant stage. Firstly, no reported Mg/S battery can exhibit acceptable specific capacity (>800 mA h g^{-1}) or withstand more than 100 charge–discharge cycles. The electrolytes that were used are deemed to be primarily responsible for the failure of cycling because of their low Mg stripping/plating efficiency, corrosiveness to inactive components (such as current collectors), and/or the formation of passivation layers on Mg anodes. Secondly, current Mg/S batteries cannot be charged and discharged at high rates. The highest charge–discharge current rate was reported to be merely $\sim$160 mA g^{-1} by Zhao-Karger *et al.*, at which a reversible discharge capacity of only 200 mA h g^{-1} was retained after 100 cycles.[17] The sluggish transformation of low-conductivity sulfur molecules into the final discharge products, namely, MgS_2/MgS, principally contributes to the poor rate capability of Mg/S batteries. In addition, the ionic conductivity, viscosity and ability to dissolve polysulfides of Mg-ion electrolytes play important roles in controlling the electrode reaction kinetics. Thirdly, Mg/S batteries exhibit high charge–discharge overpotentials (>1.0 V) and overcharge behavior and thus have extremely low Coulombic efficiencies. It is easy to conclude from the previous literature that few Mg/S batteries exhibited a high charge–discharge efficiency of up to 90%. Several reports have proposed that both the motion of multivalent species and the electrochemical conversion of the final discharge product MgS to magnesium polysulfides suffer from high kinetic barriers. Polysulfide shuttle behavior might be one contribution to overcharge behavior and low charge–discharge efficiency. The principal reason might be the decomposition of the electrolyte and/or the corrosion of the current collector, in particular when cells are charged beyond 2.5 V *vs.* Mg. Finally, Mg/S batteries exhibit varied voltage profiles when different Mg-ion electrolytes are employed, which indicates the key role of the electrolyte in the functioning of Mg/S batteries. At the current stage, the discovery of suitable Mg-ion electrolytes is still the major task for further improvements in the performance of Mg/S batteries.

Several works have already demonstrated that Mg-ion electrolytes based on a non-nucleophilic anionic species, namely, the tetrakis(hexafluoroisopropyl)borate anion ($[B(HFP)_4]^-$) display promising electrochemical properties.[16,17] The dissolution of $Mg[B(HFP)_4]_2$ in glyme forms solvated $[Mg(DME)_3]^{2+}$ cations and $[B(HFP)_4]^-$ anions. Although this electrolyte system exhibits high anodic stability up to 3.5 V *vs.* Mg, it needs rigorous synthetic and/or electrochemical procedures. Facile synthetic protocols are highly desired. In addition, Mg/S batteries using pure $Mg[B(HFP)_4]_2$ salt display unsatisfactory capacity retention (capacity of less than 300 mA h g^{-1} after 30 cycles) and overcharge behavior, which might be ascribed to the relatively high overpotentials (typically higher than 200 mV) in the Mg plating process, as well as changes in the electroactive species observed in previous works.[16]

To fundamentally address the reliability, cycle life and rate capability of Mg/S cells, we here investigate a new organic magnesium borate-based (OMBB) electrolyte system containing the solvated tetranuclear Mg-containing species $[Mg_4Cl_6(DME)_6]^{2+}$ and the $[B(HFP)_4]^-$ anion *via* the one-step *in situ* reaction of tris(hexafluoroisopropyl)borate $[B(HFP)_3]$, $MgCl_2$ and Mg powder in DME. It is well known that active cationic species undergo a conversion process to form metallic Mg crystals, which has a

pronounced effect on the Mg stripping/plating efficiency, the measured current density and the overpotential. A unique tetranuclear cationic complex, namely, $[Mg_4Cl_6(DME)_6]^{2+}$ was initially identified and was demonstrated to display high Mg plating/stripping reversibility. The replacement of mononuclear $[Mg(DME)_3]^{2+}$ by the tetranuclear $[Mg_4Cl_6(DME)_6]^{2+}$ cation would inevitably alter the steric and electronic environments. The larger tetranuclear complex needs less additional energy to undergo desolvation during the Mg plating process, which is known to be the kinetic controlling process in the formation of Mg deposits.[18] In addition, the introduction of $MgCl_2$ not only causes ligand exchange between Cl^- ions and the DME solvent to form a more thermodynamically stable cation but also has a positive effect on the electrolyte components by minimizing stability-limiting and electrochemically inactive species. As was expected, key parameters, including the ionic conductivity and overpotential during the plating process, were dramatically improved in comparison with our previous work by a factor of almost 5.[16] Impressively, a fully reversible Mg/S cell was demonstrated to withstand more than 100 cycles without obvious capacity decay and achieved a maximum charging current rate of 500 mA g^{-1}. To the best of our knowledge, these are the best results that have been achieved with respect to Mg/S batteries. Our findings convincingly validate the pivotal role of the newly designed non-nucleophilic Mg-ion electrolyte for practical Mg/S battery chemistry.

Experimental section

Synthesis of electrolyte solution

All synthesis experiments were conducted in an argon-filled glovebox with moisture and oxygen concentrations of less than 0.1 ppm at room temperature. Anhydrous tetrahydrofuran (THF, Sigma-Aldrich, 99.9%), anhydrous 1,2-dimethoxyethane (DME, Sigma-Aldrich, 99.9%), anhydrous diglyme (Aladdin, 99.5%), tris(hexafluoroisopropyl)borate [$B(HFP)_3$, TCI, 95%], anhydrous magnesium chloride ($MgCl_2$, Macklin, 99.99%), magnesium powder (Mg, Alfa, 99.8%) and *n*-hexane (Aladdin, >99.5%) were used as received. Tetraglyme (Aladdin, 99%) was dried under vacuum at 120 °C for 24 h and stored over activated 4 Å molecular sieves. OMBB electrolytes were synthesized in a vial by the simple reaction of $B(HFP)_3$, $MgCl_2$ and Mg powders in an ether solvent: firstly, $B(HFP)_3$ and $MgCl_2$ with different molar ratios were dissolved in highly pure THF, DME, diglyme or tetraglyme, and then excess Mg powder was poured into the abovementioned solution. The resulting solution was stirred for 24 hours at room temperature. A clear solution of an OMBB electrolyte was obtained after filtering unreacted Mg powder.

A 0.9 M Mg-HMSD-based electrolyte,[13] a 0.7 M $MgCl_2$ + $AlCl_3$-based electrolyte,[19] a 0.5 M $Mg[B(HFP)_4]_2$-based electrolyte[17] and a BCM-based electrolyte[16] were prepared according to previously published works.

Crystallography of equilibrium species

To identify the equilibrium species in the OMBB electrolytes, a single crystal was generated *in situ* by the slow diffusion of hexane into the clear electrolyte at room temperature. The detailed measurements and characterization data are included in the ESI.† CCDC 1545755 corresponds to $[Mg_4Cl_6(DME)_6][B(HFP)_4]_2$, 1582813 corresponds to $[Mg_2Cl_3(THF)_6][B(HFP)_4]$, 1582814 corresponds to $[Mg_2Cl_2(DME)_4][AlCl_4]_2$, and 1582815 corresponds to $[Mg_2Cl_3(THF)_6][HMDS_2AlCl_2]\cdot THF$.†

Spectral studies

NMR analyses were conducted using a Bruker AV400 spectrometer. ^1H and ^{13}C NMR spectra were referenced to the resonance of the deuterated reagent (deuterated DMSO), and ^{11}B NMR spectra were referenced to an external saturated borate solution. Electrospray ionization-mass spectrometry (ESI-MS) measurements were performed using a high-definition mass spectrometer (HDMS) equipped with an atmospheric ionization electrospray source (Agilent 1290 UPLC/6540 QTOF).

Materials characterization

Scanning electron microscopy (SEM) and energy-dispersive spectrometry (EDS) experiments were carried out with a field-emission scanning electron microscope (Hitachi S-4800). Powder X-ray diffraction (PXRD) measurements were performed with a Bruker D8 Advance diffractometer (Cu Kα radiation). Simultaneous thermogravimetric analysis-differential scanning calorimetry (TGA-DSC) measurements were performed with a TGA/DSC 3+ analyzer (SF). X-ray photoelectron spectroscopy (XPS) analysis was performed with a PerkinElmer PHI 550 spectrometer with Al Kα (1486.6 eV) as the X-ray source.

Electrochemical tests

Cyclic voltammetry (CV) was carried out using a Biologic VMP-300 potentiostat with a two-electrode cell comprising Cu foil as the working electrode and Mg foil as the counter electrode at a scan rate of 5 mV s^{-1} or 10 mV s^{-1}. Coulombic efficiencies and onset potentials for plating were calculated using previously described methods.[20] Linear sweep voltammetry was performed using the Biologic VMP-300 potentiostat with a three-electrode cell comprising different working electrodes (copper, stainless steel, aluminum, graphite film, and platinum) and Mg foil as the counter and reference electrodes at a scan rate of 1 mV s^{-1}. Experiments on the electrochemical deposition of magnesium and galvanostatic discharge–charge measurements were carried out using a LAND CT2001A system. Electrochemical impedance spectroscopy (EIS) experiments were conducted using the Biologic VMP-300 potentiostat with a frequency selected in the range from 1 MHz to 1 Hz.

The preparation of the cathodes, including Mo_6S_8, S-amorphous mesoporous carbon composites (S-AMC), S-ordered mesoporous carbon composites (S-CMK3) and S-carbon nanotube composites (S-CNT), and details of the cell assembly are presented in the ESI.† All cell assembly experiments were conducted in an argon-filled glovebox with moisture and oxygen concentrations of less than 0.1 ppm at room temperature.

Results and discussion

Analysis of equilibrium species

In order to determine the optimized composition of the OMBB electrolyte, a series of OMBB electrolytes with varying amounts of $MgCl_2$ were prepared, in which DME was used as the electrolyte solvent. The concentration of $B(HFP)_3$ was fixed at 0.5 M, and Mg powder was used in excess. The magnesium plating/stripping behavior was investigated by CV, and the results are presented in Fig. S1 and S2 (ESI†). Table S5 (ESI†) summarizes the key parameters of the Mg plating/stripping process for OMBB electrolytes with different ratios of $B(HFP)_3$: $MgCl_2$, including the plating overpotential, the oxidation peak current and the Coulombic efficiency. When the ratio of $B(HFP)_3$: $MgCl_2$ was 2 : 1, the plating overpotential was the lowest (−0.11 V *vs.* Mg/Mg^{2+}), the oxidation peak current was the highest (25.3 mA) and the Coulombic efficiency was the highest (98.67%) in the 50th CV cycle. Therefore, the optimal ratio of $B(HFP)_3$: $MgCl_2$ in the OMBB electrolyte is 2 : 1. The following characterizations and tests are specific to the electrolyte with a ratio of $B(HFP)_3$: $MgCl_2$ of 2 : 1, which is referred to as the 0.5 M OMBB electrolyte. The solvent in the 0.5 M OMBB electrolyte is specified as DME, unless noted otherwise.

To identify the equilibrium species in the 0.5 M OMBB electrolyte, transparent single crystals were obtained by the slow diffusion of hexane into the clear electrolyte at room temperature. The crystal structure of $[Mg_4Cl_6(DME)_6][B(HFP)_4]_2$ was determined by single-crystal X-ray diffraction, which revealed a complex cation consisting of four octahedrally coordinated Mg centers, six Cl atoms and six DME solvent ligands. As shown in Fig. 1, each Mg center is linked to another center by two bridging chlorine atoms, the two remaining sites on each middle Mg center are occupied by one DME molecule coordinated through two oxygen atoms, and the four remaining sites on both lateral Mg centers are occupied by two DME molecules coordinated through four oxygen atoms. In comparison with the usual $[MgCl(THF)_5]^+$ or $[Mg_2Cl_3(THF)_6]^+$ ions in APC electrolytes,[21] $[Mg_4Cl_6(DME)_6]^{2+}$ is for the first time reported to be an equilibrium cation that enables reversible Mg plating/stripping. The counter anion is composed of a boron atom and four tetrahedrally coordinated hexafluoroisopropyl groups. Besides single-crystal X-ray diffraction, the mass spectrum and NMR spectrum of the 0.5 M OMBB electrolyte were also investigated to analyze the chemical environments and equilibrium components. In Fig. S3 (ESI†), the mass spectroscopy analysis shows an exact mass-to-charge ratio that is consistent with $[B(HFP)_4]^-$, which demonstrates that the main anionic species is $[B(HFP)_4]^-$ in the 0.5 M OMBB electrolyte. In Fig. S4 (ESI†), the ^{11}B NMR spectra of pristine THFPB dissolved in DME and the 0.5 M OMBB electrolyte display a single high-intensity peak at δ = 17.17 ppm and δ = 1.27 ppm, respectively. According to the literature,[6] the chemical shift of four-coordinated boron should be less than that of three-coordinated boron, which agrees with the results of our tests. In particular, in the ^{11}B NMR spectrum of the 0.5 M OMBB electrolyte, the peak signal of $B(HFP)_4^-$ at δ = 1.27 ppm is unique, and the peak signal at δ = 17.17 ppm corresponding to THFPB has completely disappeared,

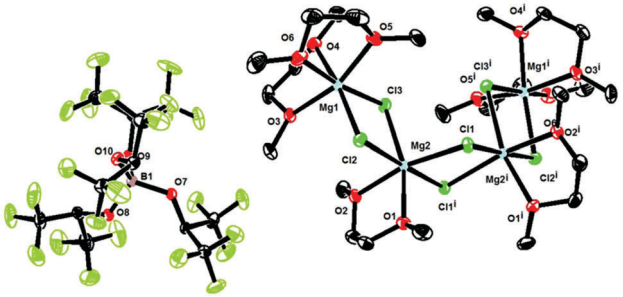

Fig. 1 ORTEP plot (50% thermal probability ellipsoids) of the molecular structure of crystalline $[Mg_4Cl_6(DME)_6][B(HFP)_4]_2$. Hydrogen atoms are omitted for clarity.

which indicates a high conversion rate from three-coordinated boron to four-coordinated boron in the process of electrolyte synthesis. In Fig. S4c (ESI†), the ^{11}B NMR spectrum of $[Mg_4Cl_6(DME)_6][B(HFP)_4]_2$ that was redissolved in the electrolyte displays a high-intensity peak at the same chemical shift as that of the pristine 0.5 M OMBB electrolyte (δ = 1.27 ppm), which confirms the uniformity of the four-coordinated boron anion before and after crystallization.

The abovementioned tetranuclear cationic complex $[Mg_4Cl_6(DME)_6]^{2+}$ was initially identified, which is distinct from the common $[Mg_2Cl_3(THF)_6]^+$ ion (Fig. S5 and Table S4, ESI†) reported in works by Muldoon *et al.* Here, we investigated the pronounced effects of both solvents and counter anions on the formation of specific organo–Mg cations by replacing DME with THF and replacing the $[B(HFP)_4]^-$ anion with the common $[AlCl_4]^-$ anion, respectively. It has been experimentally observed (Fig. S6 and Table S2, ESI†) that when OMBB electrolytes are prepared in THF solvents the common $[Mg_2Cl_3(THF)_6]^+$ species is obtained, which illustrates that donor ligands of different ethereal solvents play a crucial role in the formation of organomagnesium-based cations. Similarly, the single-crystal XRD results (Fig. S7 and Table S3, ESI†) demonstrate that the counter anion species also greatly influence the formation of the cation species. It can be concluded from the abovementioned results that both DME solvent molecules and bulky $[B(HFP)_4]^-$ counter anions play critical roles in the formation of the active tetranuclear $[Mg_4Cl_6(DME)_6]^{2+}$ cationic complex, which is expected to display superior Mg plating/stripping properties.

Characterization of 0.5 M OMBB electrolyte

At first, the magnesium plating/stripping properties of the 0.5 M OMBB electrolyte were investigated *via* extended CV cycling. As shown in Fig. 2a, the first cycle displayed a relatively higher overpotential and lower peak current density. During the following 50 cycles, the 0.5 M OMBB electrolyte exhibited a gradual increase in peak current density and a decrease in overpotential, both of which remained stable for the remaining cycles. The corresponding Coulombic efficiencies are displayed in Fig. 2b, which shows the same trend as that in the oxidation peak current density. The initial CV cycle displayed a lower efficiency of 88.64%, but the Coulombic efficiency increased to greater than 98% after 20 cycles and maintained high

reversibility over hundreds of plating/stripping cycles. The reasons for these improvements in performance may be complicated and are probably due in part to self-conditioning of the electrolyte, the breakdown of the passivation layer on the magnesium metal surface, or the presence of slight amounts of water in the electrolyte.[19,22,23] The Mg plating/stripping efficiency of the OMBB electrolytes was observed to be approximately 98.5%. For most organo-Mg cations, complicated deposition of Mg occurs *via* multiple stages of electrocrystallization mechanisms. In this respect, we assume that the moderate Coulombic efficiencies might be due to the presence of a small amount of "dead" Mg-containing insoluble films adsorbed on the Mg anodes and/or the glass fibre membrane, which has a larger specific area. In addition, the Mg plating/stripping performance of the OMBB electrolytes was also examined in non-volatile diglyme and tetraglyme, as shown in Fig. S8 (ESI†), which indicates that the OMBB electrolyte system has a wide tolerance of ethereal solvents.

The electrochemical oxidation stability of the 0.5 M OMBB electrolyte was further investigated by linear sweep voltammetry using different working electrode materials. As illustrated in Fig. 3, the oxidation onset potential was determined at the point where the change in the slope of the potential curve was greatest, which corresponds to the first maximum of the second derivative of the curve.[8] The 0.5 M OMBB electrolyte exhibited a high oxidation stability limit of up to 3.3 V *vs.* Mg/Mg^{2+} on the Pt electrode, although it displayed relatively lower anodic stability on the Al (~3.0 V *vs.* Mg/Mg^{2+}), GF (~2.8 V *vs.* Mg/Mg^{2+}), SS (~2.5 V *vs.* Mg/Mg^{2+}) and Cu (~2.0 V *vs.* Mg/Mg^{2+}) electrodes, which was principally due to the electrochemical corrosiveness of the chloride-containing 0.5 M OMBB electrolyte to non-noble metals. The non-noble metal Al had higher oxidation stability, which was probably because the passivation layer formed on the surface of the working electrode by the anodic reactions of the 0.5 M OMBB electrolyte made further anodic decomposition more difficult.[23] In comparison with monocarborane Mg salts and the $Mg[B(HFP)_4]_2$ salt, which have high anodic stabilities,[17,24] the 0.5 M OMBB electrolyte was prepared directly *in situ* from commercially available starting materials using a simple stirring approach, of which the superiority was noticeable.

Symmetric Mg//0.5 M OMBB//Mg cells were assembled to investigate the polarization properties of the 0.5 M OMBB electrolyte. As shown in Fig. 4a, the overpotential was low

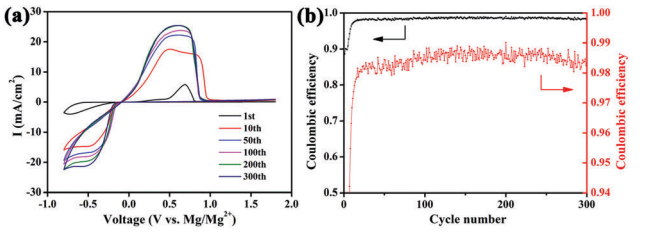

Fig. 2 (a) Cyclic voltammograms for a Cu electrode in the 0.5 M OMBB electrolyte obtained at a scanning rate of 10 mV s^{-1} in the potential range of −0.8 V to 1.8 V *vs.* Mg/Mg^{2+} over 300 cycles. (b) Corresponding Coulombic efficiency for the plating/stripping process in each cycle.

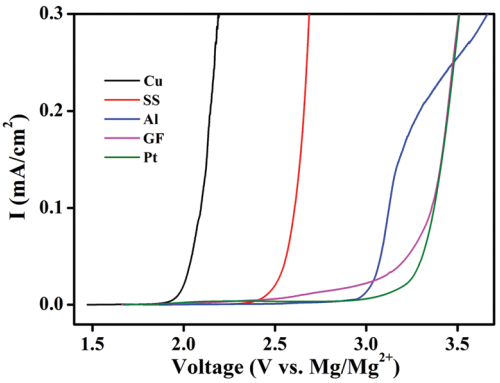

Fig. 3 Linear sweep voltammograms for the 0.5 M OMBB electrolyte at a scan rate of 1 mV s^{-1} with different working electrodes: copper (Cu, black), stainless steel (SS, red), aluminum (Al, blue), graphite film (GF, pink), and platinum (Pt, green). The counter and reference electrodes are Mg metal.

at ~0.07 V at a current density of 0.1 mA cm^{-2} and underwent a slight growth with an increase in the applied current density from 0.1 mA cm^{-2} to 1 mA cm^{-2}. Fig. 4b shows that the cell could be cycled for 700 hours with no significant increase in polarization at a current density of 0.1 mA cm^{-2}. These data indicate the outstanding stability and excellent polarization properties of the 0.5 M OMBB electrolyte. To further confirm the Mg-ion conductivity of the 0.5 M OMBB electrolyte, the ionic conductivity was determined to be 5.58 mS cm^{-1} at room temperature (see the ESI† for details of the test), which is higher than the values of other Mg electrolytes at the same concentration.[8,24–26]

To confirm the non-dendritic nature of electrochemical deposits from the 0.5 M OMBB electrolyte, their morphology and composition were investigated *via* SEM and PXRD. The PXRD result (Fig. 5a) and EDS spectrum (Fig. 5b) confirm that the agglomerated deposits essentially comprised Mg polycrystals. Magnesium metal with a hexagonal lattice was deposited onto a fresh Cu electrode at a constant current density of 0.5 mA cm^{-2} for 10 hours. The typical SEM images in Fig. 5c and d show that the Mg deposits were characterized by a dendrite-free morphology with an agglomerated hexagonal structure.

In general, the non-nucleophilic characteristics of Mg electrolytes depend on the chemical nature of the anions in the

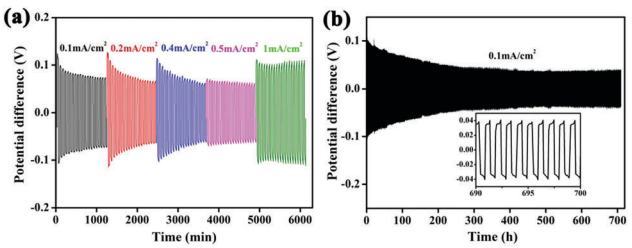

Fig. 4 (a) Polarization properties of Mg/Mg symmetrical cells with the 0.5 M OMBB electrolyte at current densities of 0.1, 0.2, 0.4, 0.5, and 1 mA cm^{-2}. (b) Long-term cycling behavior of Mg/Mg symmetrical cells with the 0.5 M OMBB electrolyte at a current density of 0.1 mA cm^{-2}. The inset shows the potential profiles from 690 h to 700 h. The cycling time was 1 h per cycle (30 min charging and 30 min discharging).

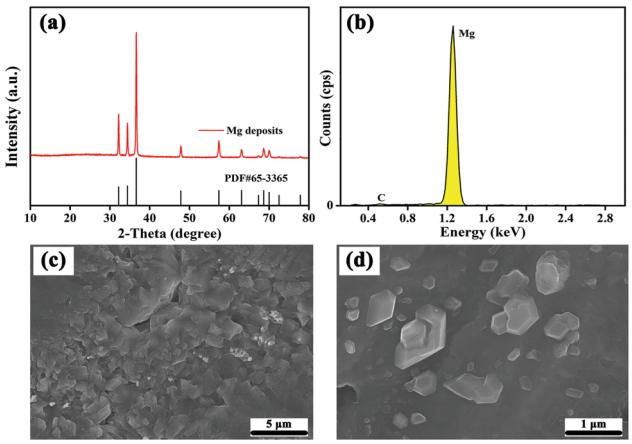

Fig. 5 (a) PXRD result and (b) EDS analysis of the Mg deposits. (c and d) Typical SEM images of the Mg deposits at different magnifications.

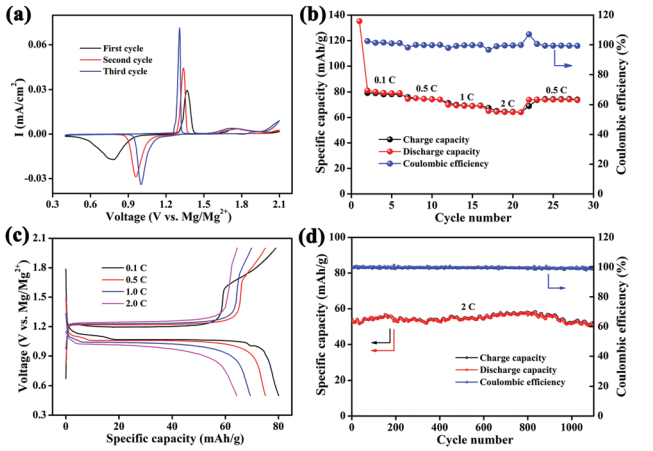

Fig. 6 Electrochemical characterization of Mo_6S_8/Mg batteries with the 0.5 M OMBB electrolyte: (a) initial three CV curves; (b) specific capacity at different charge–discharge C-rates; (c) galvanostatic charge–discharge profiles at different C-rates; (d) cycling stability and corresponding Coulombic efficiency for 1200 cycles at 2C.

Mg salts.[5,13,26,27] To confirm the non-nucleophilic characteristics of the 0.5 M OMBB electrolyte, the chemical durability of $[Mg_4Cl_6(DME)_6][B(HFP)_4]_2$ crystals with excess amounts of sulfur powder was investigated *via* ^1H, ^{13}C and ^{11}B NMR spectroscopy in deuterated DMSO. Under the same experimental conditions, the chemical shifts of these three NMR signals were identical for samples before and after the addition of sulfur powder (Fig. S9, ESI†), which indicates that no degradation or reaction between $[Mg_4Cl_6(DME)_6][B(HFP)_4]_2$ and the sulfur powder occurred. The non-reactivity of sulfur confirms the non-nucleophilic nature of $[Mg_4Cl_6(DME)_6][B(HFP)_4]_2$ crystals, which is attributed to the non-nucleophilic nature of $[B(HFP)_4]^-$ anions in the absence of reactive R^- nucleophiles.[26] Besides, the chemical inertness of the OMBB electrolyte to air and water was also demonstrated by NMR investigations (Fig. S10, ESI†), which is of great significance for future applications. The high thermal stability of $[Mg_4Cl_6(DME)_6][B(HFP)_4]_2$ crystals, as determined by TGA-DSC measurements (Fig. S11, ESI†), is also beneficial for future practical applications.

Evaluation of Mg–Mo_6S_8 and Mg–S batteries

As well as reversible magnesium plating/stripping properties, electrode–electrolyte compatibility is of vital importance for the development of practical rechargeable Mg batteries. Firstly, we evaluated the compatibility of the 0.5 M OMBB electrolyte with an Mo_6S_8 Chevrel phase cathode. 2032-Type coin batteries comprising the 0.5 M OMBB electrolyte, an Mo_6S_8 cathode, and an Mg disc anode were assembled and tested using CV measurements and the galvanostatic charge–discharge technique at room temperature. Fig. 6a shows the initial three CV curves for the Mo_6S_8/Mg batteries. The change in the overpotential was in accordance with previous works, which confirms that the initial insertion of Mg^{2+} ions into Mo_6S_8 was intrinsically slow owing to the existence of a thermodynamic barrier.[28,29] After some Mg^{2+} ions had been inserted irreversibly, the following intercalation proceeded much more rapidly. Hence, the subsequent CV cycles displayed a reduced overpotential, as some Mg^{2+} ions had been trapped during the initial cycle. Furthermore, slight self-conditioning of the 0.5 M OMBB electrolyte may also lead to a reduction in overpotential. Fig. 6b and c show the charge–discharge profiles at different C-rates (1C = 100 mA g^{-1}). The Mo_6S_8/Mg batteries exhibited excellent rate capability, and an average discharge capacity of approximately 80 mA h g^{-1} was calculated on the basis of the active mass of the cathode. These data show that a typical Mo_6S_8 electrode with the 0.5 M OMBB electrolyte displayed reasonable electrochemical Mg^{2+} storage properties in comparison with those in previous works related to Mo_6S_8/Mg batteries with an APC electrolyte.[29,30] The cycling stability of an Mo_6S_8/Mg battery was also studied, as shown in Fig. 6d, and the battery exhibited unexceptional stability over 1200 cycles with a high capacity retention of 94.4% at 2C. Although the Mo_6S_8 electrode displayed an impressive cycle life with a low capacity fade rate over prolonged cycling, it is believed to be less promising in terms of large-scale commercialization because its overall energy density is strictly limited by the low discharge voltage plateau ($\sim$1.0 V) and the low theoretical capacity ($\sim$128.8 mA h g^{-1}).

With regard to high-energy Mg battery systems, sulfur represents one of the most promising conversion cathodes owing to its high theoretical capacity (1671 mA h g^{-1} or 3459 mA h cm^{-3}) and moderate voltage plateau (1.5–2.0 V). The electrochemical properties of Mg/S batteries in the 0.5 M OMBB electrolyte were examined with different sulfur-carbon composite cathodes (including S-AMC, S-CNT and S-CMK3 composites). As shown in Fig. 7a, the S-CNT cathode exhibited the highest discharge–charge specific capacity of up to 1247 mA h g^{-1} among the abovementioned sulfur-carbon composite cathodes at a current rate of 160 mA g^{-1}, which may originate from the excellent conductivity and wetting properties of carbon nanotubes. It is worth mentioning that the S-CNT cathode maintained a capacity retention of 80.4% after 100 cycles and delivered a capacity of 1019 mA h g^{-1} in the 100th cycle. Among these sulfur-carbon composite cathodes, there was a general

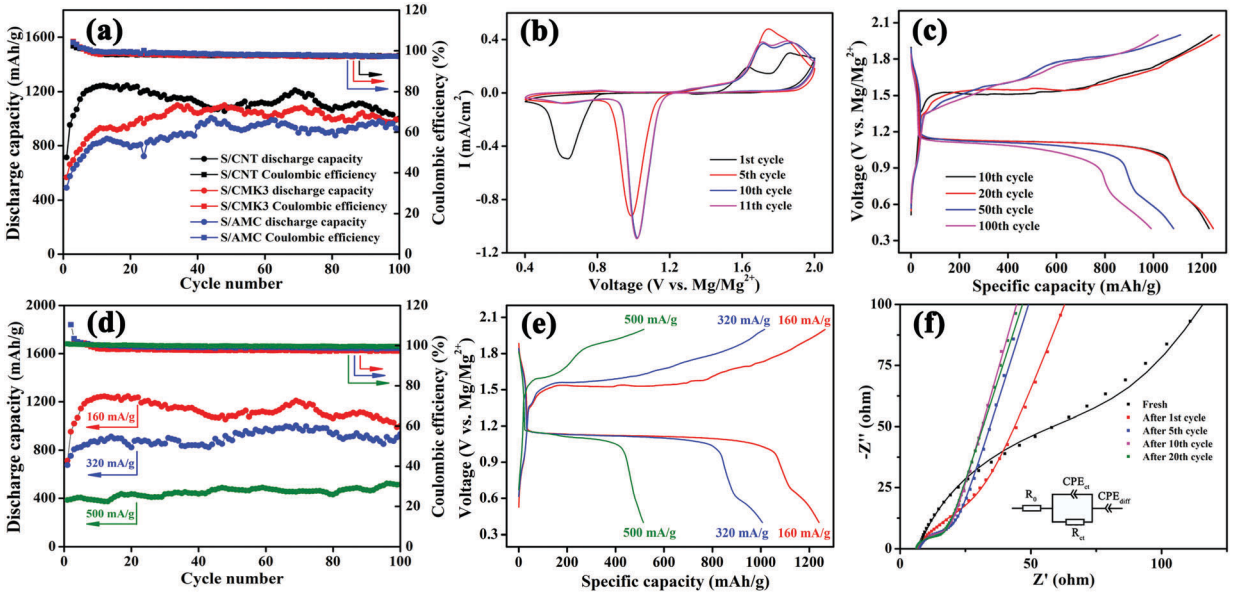

Fig. 7 (a) Discharge capacities and Coulombic efficiencies as a function of the cycle number for different S-C composite cathodes at a current rate of 160 mA g^{-1} in the 0.5 M OMBB electrolyte. (b)–(f) Electrochemical characterization of the Mg/S-CNT battery in the 0.5 M OMBB electrolyte: (b) CV curves; (c) galvanostatic charge–discharge profiles for different cycles at a current rate of 160 mA g^{-1}; (d) discharge capacities and Coulombic efficiencies at different charge–discharge current rates; (e) galvanostatic charge–discharge profiles at different charge–discharge current rates; (f) EIS measurements after different cycles (charge–discharge at a current rate of 160 mA g^{-1}). The colored points represent the results of the tests, and the colored lines are the corresponding fitting curves.

gradual improvement in the specific capacity over the first few cycles, which was probably due to self-conditioning of the 0.5 M OMBB electrolyte and slow penetration of the electrolyte into the sulfur-carbon composite cathodes.[12,16] Typical CV curves for the Mg/S-CNT battery are presented in Fig. 7b. During the first cyclic scan, only one reduction peak was present at 0.62 V, but two main oxidation peaks were observed at 1.64 V and 1.86 V, respectively. After ten cycles, the intensity of the reduction peak at 0.62 V was markedly reduced and the main reduction peak was present at 1.02 V, which indicates that the overpotential of the reduction reaction at the sulfur cathode was significantly reduced. Galvanostatic charge–discharge profiles for the Mg/S-CNT battery are presented in Fig. 7c. Obviously, both the discharge profile and the charge profile exhibit two voltage plateaus, which are consistent with the CV curves shown in Fig. 7b. To investigate the rate capability of the Mg/S-CNT battery, the cycling stability of the Mg/S-CNT battery was tested at different current densities. The discharge capacity and Coulombic efficiency as a function of the cycle number at different current densities are presented in Fig. 7d. The Mg/S-CNT battery exhibited a discharge capacity of approximately 500 mA h g^{-1} even at a higher current rate of 500 mA g^{-1}, which is the best experimental result among those reported in the literature thus far.[16] The rate capabilities of the Mg/S-AMC battery and Mg/S-CMK3 battery are presented in Fig. S12 and S13 (ESI†), respectively, and their performance was similar to that of the Mg/S-CNT battery. The voltage–capacity profiles of the Mg/S-CNT battery at different current rates are presented in Fig. 7e. Two charge voltage plateaus are still obvious at these three current rates, but at a current rate of 500 mA g^{-1} the lower discharge voltage plateau is not obvious, which is probably due to the low conductivity of the deep discharge products (*e.g.*, MgS).[31] To investigate the reasons for the improvement in specific capacity over the first few cycles, the electrochemical kinetics of the Mg/S-CNT battery before and after cycling was studied *via* EIS measurements (Fig. 7f). In the equivalent circuit, R_0 represents the bulk resistance and R_{ct} is the charge transfer resistance, whereas CPE_{ct} represents the corresponding constant phase element for the double-layer capacitance.[32] The low-frequency region cannot be modeled properly by a finite Warburg element. On the basis of previous studies,[33,34] CPE_{diff} was chosen to replace the finite diffusion element, which allowed us to obtain a good agreement with the experimental data. The fitted values of R_0, R_{ct}, CPE_{ct} and CPE_{diff} after different charge–discharge cycles are summarized in Table S6 (ESI†). After the first few cycles, R_{ct} underwent a drastic decrease, which is sure to play an important role in increases in the capacity of Mg/S-CNT batteries.[31]

It is worth noting that some by-products might exist in the OMBB electrolyte formed *in situ*. Here, in order to exclude impacts of these by-products on the properties of Mg/S batteries, the charge–discharge behavior and cycling performance of an Mg/S battery using a crystalline electrolyte containing 0.2 M $[Mg_4Cl_6(DME)_6][B(HFP)_4]_2$ in a DME solvent were investigated. Firstly, reversible Mg plating/stripping processes could be observed *via* CV measurements (Fig. S14, ESI†) when this crystalline electrolyte was used, which illustrates the feasibility of using $[Mg_4Cl_6(DME)_6][B(HFP)_4]_2$ as the active salt in Mg electrolytes. Furthermore, as demonstrated in Fig. S15 (ESI†), an Mg/S battery can also function well in the crystalline electrolyte, which compellingly demonstrates the critical role

of the proposed effective anion and cation species in the OMBB electrolyte in enhancements in the performance of Mg/S batteries.

To investigate the polysulphide shuttle phenomenon during the charge–discharge process, analyses of cycled batteries were conducted using SEM imaging and EDS mapping. SEM images and the corresponding EDS mapping of the fresh electrodes and the electrodes in a nearly full charge state at 2 V after 100 cycles are presented in Fig. 8. Obvious changes in the surface of the Mg anode can be observed between Fig. 8a and b after 100 cycles. It should be noted that the surface of the Mg anode after cycling was still dendrite-free. The morphology of the S-CNT cathode also changed dramatically after 100 cycles, as shown in Fig. 8d and e. Although the skeleton structure of the CNTs was basically unchanged, a large amount of sulfur has flowed from the interior to the surface of CNTs during the charge–discharge process to form small particles of MgS or insoluble magnesium polysulfides on the surfaces of the CNTs and the electrode voids. As seen in Fig. 8c and f, sulfur element was detected on the Mg anode and magnesium element was detected on the S-CNT cathode after 100 cycles, which indicates that polysulphides diffused from the cathode to the Mg anode during the cycling process and that the deep discharge products (*e.g.*, MgS) in the cathode were difficult to break down completely during the charge process, respectively.[31] Moreover, the S 2p spectra recorded for the cycled Mg anode, as shown in Fig. S21c (ESI†), indicate that insoluble MgS formed on the surface of the Mg anode, which further proves the existence of the notorious polysulfide shuttle effect during the cycling process.

It is well known that the notorious polysulfide shuttle phenomenon and the formation of non-electroactive MgS inorganic products could impair the cycling performance of Mg/S batteries. In our work, these problematic issues also existed, as evidenced by EDS and XPS results (Fig. 8c and Fig. S21c, ESI†). Interestingly, the Mg–S batteries in our present work displayed only a slight decay in capacity or even an increase after long-term cycling (as shown in Fig. 7d). Here, we assume that two critical factors were responsible for the excellent cycling performance observed in this work. Firstly, the active anion and cation species in specific electrolytes are believed to play key roles in enhancing the electrochemical performance of Mg/S batteries. It has been experimentally demonstrated (Fig. S16–S19, ESI†) that Mg/S batteries that used the OMBB electrolyte outperformed all Mg/S systems that used previously reported non-nucleophilic electrolytes (including the Mg-HMDS-based electrolyte, $MgCl_2$ + $AlCl_3$-based electrolyte, $Mg[B(HFP)_4]_2$-based electrolyte and BCM-based electrolyte) in terms of specific capacity and rate capability, as well as cycling performance, which highlights the development and significance of the newly investigated OMBB electrolyte. Secondly, our preliminary research on the charge storage mechanism of Mg/Se batteries shows that copper in the current collector may help to activate the sluggish reactions of MgSe discharge products and immobilize polyselenides by forming intermediates.[35] The utilization of Cu current collectors might be beneficial for enhancements in specific capacity and capacity retention in our present system. In fact, NuLi *et al.* have recently presented the interesting conclusion that a sulfur cathode can be made compatible with traditional nucleophilic APC-based electrolytes (*e.g.*, the $(PhMgCl)_2$–$AlCl_3$/THF electrolyte) for Mg/S batteries by using a Cu current collector instead of SS and graphite current collectors.[36] They have demonstrated that Cu chemically stabilizes S by forming copper sulfides, and the strong interaction between Cu and S in copper sulfides protects sulfur from the electrolyte and increases the compatibility of

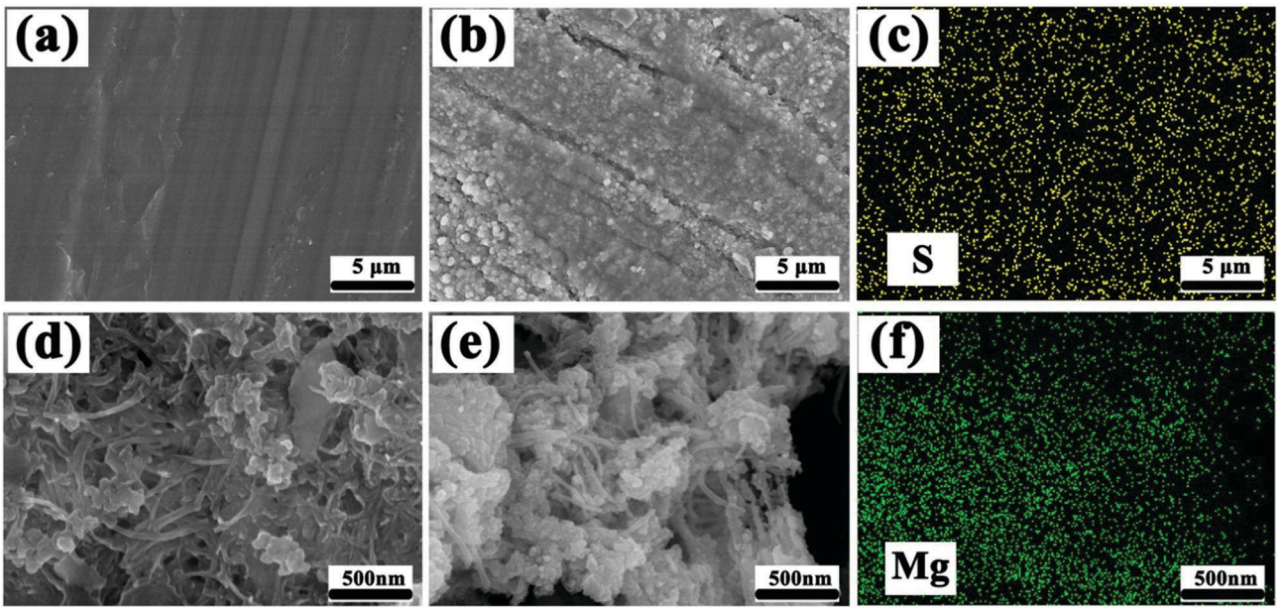

Fig. 8 Typical SEM images of (a) the fresh Mg anode and (b) the Mg anode in a nearly full charge state at 2 V after 100 cycles. (c) Elemental map corresponding to sulfur in the region shown in (b). Typical SEM images of (d) the fresh S-CNT cathode and (e) the S-CNT cathode in a nearly full charge state at 2 V after 100 cycles. (f) Elemental map corresponding to magnesium in the region shown in (e).

Table 1 Comparison of electrochemical properties of reported Mg/S battery systems

Electrolyte	Sulfur cathode	Maximum specific capacity/mA h g^{-1}	Charge–discharge rate	Overpotential/V	Cycling stability
HMDSMgCl + $AlCl_3$[5]	S-Carbon black	230	50 μA	>1.0	Only 32% of initial capacity in the second cycle
$Mg(TFSI)_2$[14]	S-CMK3	~250	~30 mA g^{-1}	>1.0	Only 4 charge–discharge cycles with a specific capacity of about 250 mA h g^{-1}
$[Mg(THF)_6][AlCl_4]_2$[15]	S-Nitrogen-doped graphene	700	~17 mA g^{-1}	>1.5	20 charge–discharge cycles with capacity retention of 10%
Mg-HMDS + LiTFSI[12]	S-Activated carbon cloth	1000	71 mA g^{-1}	~1.0	30 charge–discharge cycles with obvious overcharge phenomenon
$(HMDS)_2Mg$ + $AlCl_3$[13]	S-CMK400PEG	800	20 mA g^{-1}	~0.8	20 charge–discharge cycles with capacity retention of 32.5%
$(HMDS)_2Mg$ + $AlCl_3$[37]	S-Reduced graphene oxide	1024	20 mA g^{-1}	>1.0	50 charge–discharge cycles with capacity retention of 21.4%
$(HMDS)_2Mg$ + $AlCl_3$[31]	S-Carbon nanofiber	~1100	~30 mA g^{-1}	~0.8	20 charge–discharge cycles with capacity retention of 65%
$(HMDS)_2Mg$ + $AlCl_3$[38]	SeS_2-CMK3	600	40 mA g^{-1}	N/A	Only 46.6% of initial discharge capacity in the second cycle
BCM electrolyte[16]	S-AMC	1081	50 mA g^{-1}	~0.4	30 charge–discharge cycles with capacity retention of 86.4%
$Mg[B(HFP)_4]_2$[17]	S-CMK3	~500	~160 mA g^{-1}	~0.8	100 charge–discharge cycles with capacity retention of ~40%
Our work	S-CNT	1247	160 mA g^{-1}	~0.3	100 charge–discharge cycles with capacity retention of 80.4%
		1006	320 mA g^{-1}	~0.4	
		514	500 mA g^{-1}	~0.5	

sulfur with the electrolyte. It is worth noting that with a Cu current collector the electrochemical performance of Mg/S batteries that employed APC-based electrolytes was greatly inferior to that of Mg/S batteries that used the OMBB electrolyte (after 20 cycles, 150 mA h g^{-1} for APC-based electrolytes at a current rate of 10 mA g^{-1} *vs.* 1200 mA h g^{-1} for the OMBB electrolyte at a current rate of 160 mA g^{-1}), which illustrates that the present novel OMBB electrolyte contributed to the enhancement in electrochemical properties to a very great extent. The electrochemical performance of Mg/S batteries that used Al current collectors (Fig. S20, ESI†), in combination with XPS studies of cycled sulfur cathodes from Mg/S batteries that used Cu current collectors (Fig. S21 and S22, ESI†), also demonstrate that our present Mg/S system may undergo a unique yet complicated polysulfide shuttle mechanism. More detailed descriptions and a fundamental understanding of these aspects might be beyond the scope of this work.

In comparison with those reported in all the obtainable published literature (summarized in Table 1), the Mg/S batteries that employed the OMBB electrolyte displayed significant comprehensive improvements in performance, which mainly included capacity density, rate capability, charge–discharge overpotential and cycling stability. Our work will be a critical step in promoting the practical applications of Mg/S battery systems.

Conclusions

In conclusion, a new type of organic borate-based Mg electrolyte has been developed *via* a straightforward and scalable *in situ* reaction of $B(HFP)_3$, $MgCl_2$ and Mg powder in DME. The major equilibrium species in the OMBB electrolyte have been identified *via* relevant spectral tests and crystallographic analysis and mainly comprise tetracoordinated anions $[B(HFP)_4]^-$ and solvated cations $[Mg_4Cl_6(DME)_6]^{2+}$. The resulting electrolyte consisting of $B(HFP)_3$ with the Lewis base $MgCl_2$ in a ratio of 2 : 1 displayed highly promising performance in terms of high Coulombic efficiency (greater than 98%), high ionic conductivity of 5.58 mS cm^{-1} and high oxidation stability up to 3.0 V (*vs.* Mg/Mg^{2+}) to commonly used Al foil. In addition, its perfect chemical compatibility with sulfur cathodes makes the OMBB electrolyte a very suitable candidate for Mg/S batteries with high energy density, which have for the first time been demonstrated to display a very stable discharge capacity of above 1000 mA h g^{-1} for more than 100 cycles. It should also be mentioned that, to our knowledge, Mg/S batteries assembled using the 0.5 M OMBB electrolyte achieved a maximum charging current rate of up to 500 mA g^{-1}, at which they delivered a reasonable, stable specific capacity of 500 mA h g^{-1}. This OMBB electrolyte represents a huge improvement over previously developed Grignard-based chemistries and is also competitive with HMDS-based and monocarborane-based Mg electrolytes in terms of its easy synthesis and superior Mg/S battery performance. Taking these achievements into consideration, our work could effectively promote the R&D of Mg/S batteries with high energy density.

Conflicts of interest

There are no conflicts to declare.

Acknowledgements

This work was financially supported by the National Natural Science Foundation for Distinguished Young Scholars of China

(Grant No. 51625204) and the Youth Innovation Promotion Association of CAS (2016193). The authors gratefully acknowledge Mr Zai-yong Zhang (Pharmaceutical Analytical & Solid-State Chemistry Research Center, Shanghai Institute of Materia Medica, Chinese Academy of Sciences, Shanghai 201203, China) and Dr Bingbing Chen (Qingdao Institute of Bioenergy and Bioprocess Technology, Chinese Academy of Sciences, Qingdao 266101, China) for their analysis of the crystal structures.

Notes and references

1 H. D. Yoo, I. Shterenberg, Y. Gofer, G. Gershinsky, N. Pour and D. Aurbach, *Energy Environ. Sci.*, 2013, **6**, 2265–2279.
2 J. Muldoon, C. B. Bucur and T. Gregory, *Chem. Rev.*, 2014, **114**, 11683–11720.
3 P. Saha, M. K. Datta, O. I. Velikokhatnyi, A. Manivannan, D. Alman and P. N. Kumta, *Prog. Mater. Sci.*, 2014, **66**, 1–86.
4 J. Song, E. Sahadeo, M. Noked and S. B. Lee, *J. Phys. Lett.*, 2016, **7**, 1736–1749.
5 H. S. Kim, T. S. Arthur, G. D. Allred, J. Zajicek, J. G. Newman, A. E. Rodnyansky, A. G. Oliver, W. C. Boggess and J. Muldoon, *Nat. Commun.*, 2011, **2**, 427.
6 Y.-s. Guo, F. Zhang, J. Yang, F.-f. Wang, Y. NuLi and S.-i. Hirano, *Energy Environ. Sci.*, 2012, **5**, 9100–9106.
7 M. M. Huie, D. C. Bock, E. S. Takeuchi, A. C. Marschilok and K. J. Takeuchi, *Coord. Chem. Rev.*, 2015, **287**, 15–27.
8 R. Schwarz, M. Pejic, P. Fischer, M. Marinaro, L. Jörissen and M. Wachtler, *Angew. Chem., Int. Ed.*, 2016, **55**, 14958–14962.
9 D. Aurbach, Z. Lu, A. Schechter, Y. Gofer, H. Gizbar, R. Turgeman, Y. Cohen, M. Moshkovich and E. Levi, *Nature*, 2000, **407**, 724–727.
10 X. Sun, P. Bonnick, V. Duffort, M. Liu, Z. Rong, K. A. Persson, G. Ceder and L. F. Nazar, *Energy Environ. Sci.*, 2016, **9**, 2273–2277.
11 M. Armand and J.-M. Tarascon, *Nature*, 2008, **451**, 652–657.
12 T. Gao, M. Noked, A. J. Pearse, E. Gillette, X. Fan, Y. Zhu, C. Luo, L. Suo, M. A. Schroeder and K. Xu, *J. Am. Chem. Soc.*, 2015, **137**, 12388–12393.
13 Z. Zhao-Karger, X. Zhao, D. Wang, T. Diemant, R. J. Behm and M. Fichtner, *Adv. Energy Mater.*, 2015, **5**, 1401155.
14 S.-Y. Ha, Y.-W. Lee, S. W. Woo, B. Koo, J.-S. Kim, J. Cho, K. T. Lee and N.-S. Choi, *ACS Appl. Mater. Interfaces*, 2014, **6**, 4063–4073.
15 W. Li, S. Cheng, J. Wang, Y. Qiu, Z. Zheng, H. Lin, S. Nanda, Q. Ma, Y. Xu, F. Ye, M. Liu, L. Zhou and Y. Zhang, *Angew. Chem.*, 2016, **128**, 6516–6520.
16 Z. Zhang, Z. Cui, L. Qiao, J. Guan, H. Xu, X. Wang, P. Hu, H. Du, S. Li and X. Zhou, *Adv. Energy Mater.*, 2017, **7**, 1602055.
17 Z. Zhao-Karger, M. E. G. Bardaji, O. Fuhr and M. Fichtner, *J. Mater. Chem. A*, 2017, **5**, 10815–10820.
18 N. N. Rajput, X. Qu, N. Sa, A. K. Burrell and K. A. Persson, *J. Am. Chem. Soc.*, 2015, **137**, 3411–3420.
19 S. He, J. Luo and T. L. Liu, *J. Mater. Chem. A*, 2017, **5**, 12718–12722.
20 R. Mohtadi, M. Matsui, T. S. Arthur and S.-J. Hwang, *Angew. Chem., Int. Ed.*, 2012, **51**, 9780–9783.
21 N. Pour, Y. Gofer, D. T. Major and D. Aurbach, *J. Am. Chem. Soc.*, 2011, **133**, 6270–6278.
22 C. J. Barile, E. C. Barile, K. R. Zavadil, R. G. Nuzzo and A. A. Gewirth, *J. Phys. Chem. C*, 2014, **118**, 27623–27630.
23 J. T. Herb, C. A. Nist-Lund and C. B. Arnold, *ACS Energy Lett.*, 2016, **1**, 1227–1232.
24 O. Tutusaus, R. Mohtadi, T. S. Arthur, F. Mizuno, E. G. Nelson and Y. V. Sevryugina, *Angew. Chem., Int. Ed.*, 2015, **54**, 7900–7904.
25 O. Mizrahi, N. Amir, E. Pollak, O. Chusid, V. Marks, H. Gottlieb, L. Larush, E. Zinigrad and D. Aurbach, *J. Electrochem. Soc.*, 2008, **155**, A103–A109.
26 T. Liu, Y. Shao, G. Li, M. Gu, J. Hu, S. Xu, Z. Nie, X. Chen, C. Wang and J. Liu, *J. Mater. Chem. A*, 2014, **2**, 3430–3438.
27 Z. Zhao-Karger, X. Zhao, O. Fuhr and M. Fichtner, *RSC Adv.*, 2013, **3**, 16330–16335.
28 M. Levi, E. Lancry, H. Gizbar, Z. Lu, E. Levi, Y. Gofer and D. Aurbach, *J. Electrochem. Soc.*, 2004, **151**, A1044–A1051.
29 Y. Cheng, L. R. Parent, Y. Shao, C. Wang, V. L. Sprenkle, G. Li and J. Liu, *Chem. Mater.*, 2014, **26**, 4904–4907.
30 P. Saha, P. H. Jampani, M. K. Datta, C. U. Okoli, A. Manivannan and P. N. Kumta, *J. Electrochem. Soc.*, 2014, **161**, A593–A598.
31 X. Yu and A. Manthiram, *ACS Energy Lett.*, 2016, **1**, 431–437.
32 Z. A. Ghazi, X. He, A. M. Khattak, N. A. Khan, B. Liang, A. Iqbal, J. Wang, H. Sin, L. Li and Z. Tang, *Adv. Mater.*, 2017, **29**, 1606817.
33 Q.-C. Zhuang, T. Wei, L.-L. Du, Y.-L. Cui, L. Fang and S.-G. Sun, *J. Phys. Chem. C*, 2010, **114**, 8614–8621.
34 J. Chai, Z. Liu, J. Zhang, J. Sun, Z. Tian, Y. Ji, K. Tang, X. Zhou and G. Cui, *ACS Appl. Mater. Interfaces*, 2017, **9**, 17897–17905.
35 Z. Zhang, B. Chen, H. Xu, Z. Cui, S. Dong, A. Du, J. Ma, Q. Wang, X. Zhou and G. Cui, *Adv. Funct. Mater.*, 2017, 1701718.
36 L. Zeng, N. Wang, J. Yang, J. Wang and Y. NuLi, *J. Electrochem. Soc.*, 2017, **164**, A2504–A2512.
37 B. Vinayan, Z. Zhao-Karger, T. Diemant, V. S. K. Chakravadhanula, N. I. Schwarzburger, M. A. Cambaz, R. J. Behm, C. Kübel and M. Fichtner, *Nanoscale*, 2016, **8**, 3296–3306.
38 Z. Zhao-Karger, X.-M. Lin, C. Bonatto Minella, D. Wang, T. Diemant, R. J. Behm and M. Fichtner, *J. Power Sources*, 2016, **323**, 213–219.